Theory of oxygen diffusion in the $YBa_2Cu_3O_{7-x}$ superconducting compound

Jae-Sung Choi, Mehmet Sarikaya, Ilhan A. Aksay, and Ryoichi Kikuchi*
Department of Materials Science and Engineering and Advanced Materials Technology Center, Washington Technology Centers, University of Washington, Seattle, Washington 98195
(Received 25 October 1989)

Oxygen diffusion coefficients in the $YBa_2Cu_3O_{7-x}$ superconducting compound are calculated by employing the pair approximation of the path probability method. The results show that the diffusion of oxygen in this compound is significantly dependent on the oxygen density and the degree of long-range order. It was found that the oxygen diffusion rate in the tetragonal phase is faster than that in the orthorhombic phase, with activation energies for diffusion of 0.8 and 1.2 eV, respectively, with the rate changing abruptly when the phase transformation takes place. We discuss the relationship between oxygen diffusion and each pair probability in connection with each pair's interaction energy values. The kinetics of oxygen diffusion obtained from the present model is discussed in the context of experimental values in the literature and with respect to twin boundary diffusion.

I. INTRODUCTION

The understanding of the kinetics of oxygen diffusion in $YBa_2Cu_3O_{7-x}$ is important from both scientific and technological points of view. It is essential that $YBa_2Cu_3O_{7-x}$ be produced with predictable microstructures and tailored compositional homogeneity in order to obtain the expected superconducting properties. It is already known that the tetragonal (semiconducting) to the orthorhombic (superconducting) phase transition temperature depends on the value of x in the formula of the compound[1,2] and that x can be varied during the processing of the material.[3–5] Furthermore, the properties of both the normal and the superconducting states of $YBa_2Cu_3O_{7-x}$ strongly depend on the oxygen concentration and the degree of oxygen ordering in the orthorhombic phase.[1–4,6–7] It seems, therefore, that the mechanism of superconductivity in these high-T_c oxides is related to the behavior of oxygen (ordering, interaction with Cu, etc.) in the lattice.[8]

It is now clear that just varying the "bulk" value of oxygen is not sufficient in predicting unique properties; but the gradient and distribution of oxygen within single crystals or grains of polycrystalline samples are important for understanding the properties of $YBa_2Cu_3O_{7-x}$. It is well established that the spatial distribution of oxygen is related to the local variation in $\Delta a/a$ (where $\Delta a = b - a$, and b and a are the lattice parameters of the orthorhombic phase in the [010] and [100] directions) in single crystals and polycrystals.[9–11] Other inhomogeneities, such as "shell" formation within the grains,[12] variations along the twin[13–14] and grain boundaries,[15–16] secondary ordering,[17] and transition oxide formation[18,19] within $YBa_2Cu_3O_{7-x}$ grains have also been measured and some of their effects on the properties have been established.[20,21]

In the orthorhombic lattice, the oxygen variations take place in the $a-b$ plane and in the $O(I)$ sites.[1–4,6–7] The kinetics of oxygen diffusion is also found to be different on heating to and cooling from the formation (or annealing) temperature.[22] The kinetics varies depending on the type of gas environment (air, oxygen, or other)[22–24] and the value of the oxygen partial pressure.[25]

Systematic studies on the kinetics of oxygen diffusion in $YBa_2Cu_3O_{7-x}$ under various conditions have been performed both theoretically[26] and experimentally.[22–25,27–29] In all these studies, a total bulk diffusion is taken into account and the resultant kinetic behavior of oxygen in each situation is found to be scattered. In actuality, diffusion of oxygen may take place in a hierarchical order: (i) diffusion along the surface (and surface layers), (ii) diffusion along the grain boundaries, (iii) diffusion along the twin boundaries, and (iv) lattice diffusion. The first two cases, surface and grain boundary diffusion, may greatly affect the kinetics of "in" and "out" diffusion rates which are closely related to porosity of the polycrystalline samples. These cases will not be studied in this paper. The third case may be an important mechanism for diffusion since transformation twins form in the lattice to accommodate stresses created as a result of the shape change during the tetragonal to orthorhombic transformation.[1,2,11] Twin boundaries may, therefore, act as easy diffusion paths (just like "pipe diffusion" along dislocations in metals and alloys).[30] This case is studied by us in an accompanying paper[31] and a short analysis of its consequences will be given in Sec. V of this paper. The main emphasis of the present paper is, however, the lattice diffusion of oxygen in $YBa_2Cu_3O_{7-x}$ as based on a model that shows a relationship between the oxygen diffusion rate and oxygen content. Since the structure of the oxide is quite dependent on the oxygen content and ordering, as shown in our phase diagram calculation,[32] the model describes the variation of the oxygen diffusion rate with respect to the structural features.

In the present model, the stacking sequence of $YBa_2Cu_3O_{7-x}$ layers is denoted as Y-CuO_2-BaO-CuO-BaO-CuO_2. As in the previous studies,[22–28] we can assume that oxygen diffusion takes place mainly in the

Cu-O basal plane, and atomic diffusion in the c direction is negligible. In addition, as it is assumed that the vacancy mechanism is the most likely diffusion mechanism in this system, the problem of oxygen diffusion is reduced to that of the oxygen-vacancy migration in a two-dimensional lattice plane. This model is applicable to the self-diffusion of the oxygen atoms; hence the pair approximation of the cluster variation method (CVM) (Ref. 33) and the path probability method (PPM) (Ref. 34) are applied to the calculations. In these calculations, we consider one first-nearest and two second-nearest interaction energy parameters. To our knowledge, this is the first attempt to include the second-nearest interaction energy parameters in the pair approximation of the PPM in order to achieve a more accurate picture of the kinetics of oxygen diffusion in the $YBa_2Cu_3O_{7-x}$ lattice, which would be more consistent with the experimental results in the literature.[12,22–25,27,28]

II. EQUILIBRIUM CONDITION

To examine how oxygen and vacancies are distributed over the Cu-O basal plane of $YBa_2Cu_3O_{7-x}$ in equilibrium, we employ the pair approximation of the CVM with the consideration of two different kinds of second-nearest-neighbor (NN) interaction energies in addition to the first-NN interaction as mentioned in the Introduction. The same interaction energy scheme is applied to the PPM calculations, which will be described in Sec. III.

A. Energy and state variables

Figure 1 schematically illustrates the Cu-O basal plane in the $YBa_2Cu_3O_{7-x}$ superconducting compound. Two oxygen lattice positions, α and β, are defined in this figure. Also, to designate an oxygen and a vacancy, subscripts i (or j)=1 and 2 are used, respectively. The first-NN i-j interaction energy between α and β positions is defined as $V_{1,ij}$ and the second-NN interactions are defined as $V_{2,ij}$ or $V_{3,ij}$. Here $V_{2,ij}$ is the i-j interaction by superexchange through a Cu atom and $V_{3,ij}$ is the direct i-j interaction. Although we use the general subscripts ij, we assume that a vacancy does not contribute

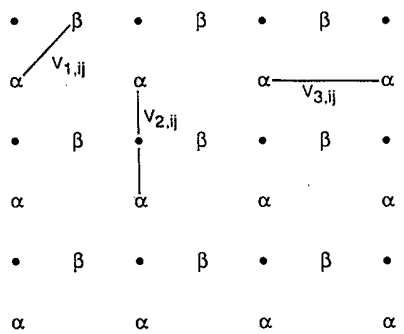

FIG. 1. Schematic diagram of the atomic distribution on the Cu-O basal plane. Three different interaction energies are defined.

TABLE I. Point variables.

$\underset{i}{\alpha}$	$x_{\alpha,i}$	$\underset{i}{\beta}$	$x_{\beta,i}$

to an interaction. Therefore $V_{1,ij}=0$ when i or j is equal to 2. A similar comment holds for $V_{2,ij}$ and $V_{3,ij}$.

For the CVM formulation, it is necessary to define the state variables. In the present study, we apply the pair approximation; the variables are defined accordingly in Tables I and II. The point variable $x_{\alpha,i}$ is the probability of finding an α lattice point that is occupied by the ith species. The pair probability y_{ij} is the probability of finding such a NN α-β pair in which i sits on the α site and j sits on the β site. Other pair variables in Table II are defined for respective site and species combinations. Note that in y_{ij} the order of the two subscripts is meaningful. The reduction relations that exist among the state variables are expressed as

$$x_{\alpha,i}=\sum_j y_{ij}=\sum_j u_{ij}=\sum_j w_{ij}\ , \tag{2.1}$$

$$x_{\beta,i}=\sum_j y_{ji}=\sum_j v_{ij}=\sum_j z_{ij}\ . \tag{2.2}$$

B. Entropy

Entropy, S, of this system is written in exponential form as

$$e^{S/k}=W_{\rm I}W_{\rm II}W_{\rm III}\ , \tag{2.3}$$

where k is the Boltzmann constant, $W_{\rm I}$, $W_{\rm II}$, and $W_{\rm III}$ are expressions for the number of ways of distributing points, with the first-NN and second-NN pairs over the lattice points, respectively, and they are written as

$$W_{\rm I}=\left[\frac{N!}{\{\alpha\}_N}\frac{N!}{\{\beta\}_N}\right]^{1/2}, \tag{2.4}$$

$$W_{\rm II}=\left[\frac{\{\alpha\}_N\{\beta\}_N}{\{\alpha\text{-}\beta\}_N N!}\right]^2, \tag{2.5}$$

$$W_{\rm III}=\left[\frac{\{\alpha\}_N\{\alpha\}_N}{\{\alpha\text{-Cu-}\alpha\}_N N!}\right]^{1/2}\left[\frac{\{\alpha\}_N\{\alpha\}_N}{\{\alpha\text{--}\alpha\}_N N!}\right]^{1/2} \times\left[\frac{\{\beta\}_N\{\beta\}_n}{\{\beta\text{-Cu-}\beta\}_N N!}\right]^{1/2}\left[\frac{\{\beta\}_N\{\beta\}_N}{\{\beta\text{--}\beta\}_N N!}\right]^{1/2}. \tag{2.6}$$

The brace notations are defined in Ref. 33.

TABLE II. Pair variables.

$\underset{i}{\alpha}\text{-}\underset{j}{\beta}$	y_{ij}
$\underset{i}{\alpha}\text{-Cu-}\underset{j}{\alpha}$	u_{ij}
$\underset{i}{\alpha}\text{-}\underset{j}{\alpha}$	w_{ij}
$\underset{i}{\beta}\text{-Cu-}\underset{j}{\beta}$	v_{ij}
$\underset{i}{\beta}\text{-}\underset{j}{\beta}$	z_{ij}

In taking the logarithm of W_{I}, W_{II}, and W_{III}, we use Stirling's approximation and write

$$S/k=\tfrac{7}{2}N\sum_i[\mathcal{L}(x_{\alpha,i})+\mathcal{L}(x_{\beta,i})]-2N\sum_{ij}[\mathcal{L}(y_{ij})] -\frac{N}{2}\sum_{ij}[\mathcal{L}(u_{ij})+\mathcal{L}(v_{ij})+\mathcal{L}(w_{ij})+\mathcal{L}(z_{ij})] . \tag{2.7}$$

Here we use the abbreviation of the $\mathcal{L}$ function defined by

$$\mathcal{L}(x)=x\ln x-x . \tag{2.8}$$

If there are no second-neighbor pairs to be taken into account, then

$$e^{S/k}=W_{\mathrm{I}}W_{\mathrm{II}}=\frac{(\{\alpha\}_N\{\beta\}_N)^{3/2}}{\{\alpha\text{-}\beta\}^2N!} . \tag{2.9}$$

In addition, if we consider only α sites, then

$$e^{S/k}=\left[\frac{N!}{\{\alpha\}_N}\right]^{1/2}W_{\mathrm{III}} =\frac{\{\alpha\}_N^{3/2}}{(\{\alpha\text{-Cu-}\beta\}_N\{\alpha\text{---}\alpha\}_N)^{1/2}N!} . \tag{2.10}$$

When we compare Eqs. (2.9) and (2.10) with the expressions in Ref. 33, we can verify that they agree, thus satisfying a necessary condition to support our present derivation of the entropy expression.

C. Grand potential

The grand potential Ω is expressed as

$$\Omega=E-TS-\mu\rho , \tag{2.11}$$

where S is the entropy shown in Eq. (2.3), and E is the total energy written as

$$E=N\sum_{ij}\left[2V_{1,ij}y_{ij}+\frac{V_{2,ij}}{2}(v_{ij}+u_{ij}) +\frac{V_{3,ij}}{2}(w_{ij}+z_{ij})\right] . \tag{2.12}$$

Here, μ and ρ are the chemical potential and the density of oxygen, respectively.

The equilibrium distribution can be obtained by minimizing Ω, and to do this, it is convenient to use the natural iteration method (NIM).[35]

III. DIFFUSION FORMULATION

To calculate the oxygen diffusion rate in the Cu-O basal plane of the $YBa_2Cu_3O_{7-x}$ structure, we apply the path probability method, which is an extension of the CVM to the time-dependent processes. The PPM follows the same statistical principles as the CVM, except that it includes the time axis. For example, analogous to the state variables in the CVM, the path variables are the basic variables in the PPM. Also, the path probability is maximized in the PPM to find the most probable path, in the same sense as the grand potential is minimized in the CVM to determine the most probable cluster configurations.

TABLE III. Point path variables. An arrow shows an example of the jump direction. The broken line means a jump outside the cluster.

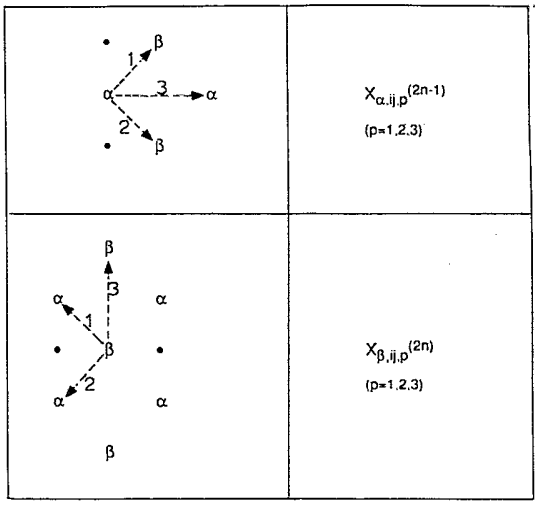

A. Path variables

The path variables are defined to specify the change occurring in the system during a time interval Δt and are written as $f(t,t+\Delta t)$ in which t and $t+\Delta t$ stand for the initial and the final time, respectively. In the present study, we introduce two levels of the path variables, i.e., the point and pair variables, which are defined in Tables III and IV. In these tables, arrows show possible jump directions. The reverse jumps are also allowed. A solid line represents a jump inside the cluster, and a broken line indicates a jump outside the cluster. Since the atomic configuration changes only when an oxygen jumps into a vacancy, the cases $Y_{12,21}$ and $Y_{21,12}$ of $Y_{ij,ji}$ are for atomic migration. Other cases $Y_{11,11}$ and $Y_{22,22}$ are also included in the formulation, but they represent the probability for no change. In $Y_{ij,ik,p}$, i ($=1$ or 2) remains the same at t and $t+\Delta t$, while j ($=1$ or 2) at t changes into k at $t+\Delta t$. Similar comments hold for the other variables also.

B. Path probability function

The path probability function $\mathcal{P}$ is composed of three factors, i.e., $\mathcal{P}=\mathcal{P}_1\mathcal{P}_2\mathcal{P}_3$, as written in the following:

$$N^{-1}\ln\mathcal{P}_1=\tfrac{7}{2}\sum_{ij,p}\mathcal{L}(X_{\alpha,ij,p})+\tfrac{7}{2}\sum_{ij,p}\mathcal{L}(X_{\beta,ij,p})-2\sum_{\text{all}}\mathcal{L}(Y_{ij,kl,p}) -\tfrac{1}{2}\sum_{\text{all}}[\mathcal{L}(U_{ij,kl,p})+\mathcal{L}(V_{ij,kl,p})+\mathcal{L}(W_{ij,kl,p})+\mathcal{L}(Z_{ij,kl,p})] , \tag{3.1}$$

$$N^{-1}\ln\mathcal{P}_2=\sum_{ij} Y_{ij,ji}[\ln(\theta_{\rm I}\Delta t)-U_{\rm I}/kT]+\sum_{ij}(W_{ij,ji}+Z_{ij,ji})[\ln(\theta_{\rm II}\Delta t)-U_{\rm II}/kT]\ , \tag{3.2}$$

and

$$N^{-1}\ln\mathcal{P}_3=\frac{1}{kT}\sum_{\rm all} V_{1,ij}(Y_{ij,ik,p}+Y_{ij,kj,p})/2+\frac{1}{kT}\sum_{\rm all} V_{2,ij}(U_{ij,ik,p}+U_{ij,kj,p}+V_{ij,ik,p}+V_{ij,kj,p})/2$$
$$+\frac{1}{kT}\sum_{\rm all} V_{3,ij}(W_{ij,ik,p}+W_{ij,kj,p}+Z_{ij,ik,p}+Z_{ij,kj,p})/2\ . \tag{3.3}$$

TABLE IV. Pair path variables.

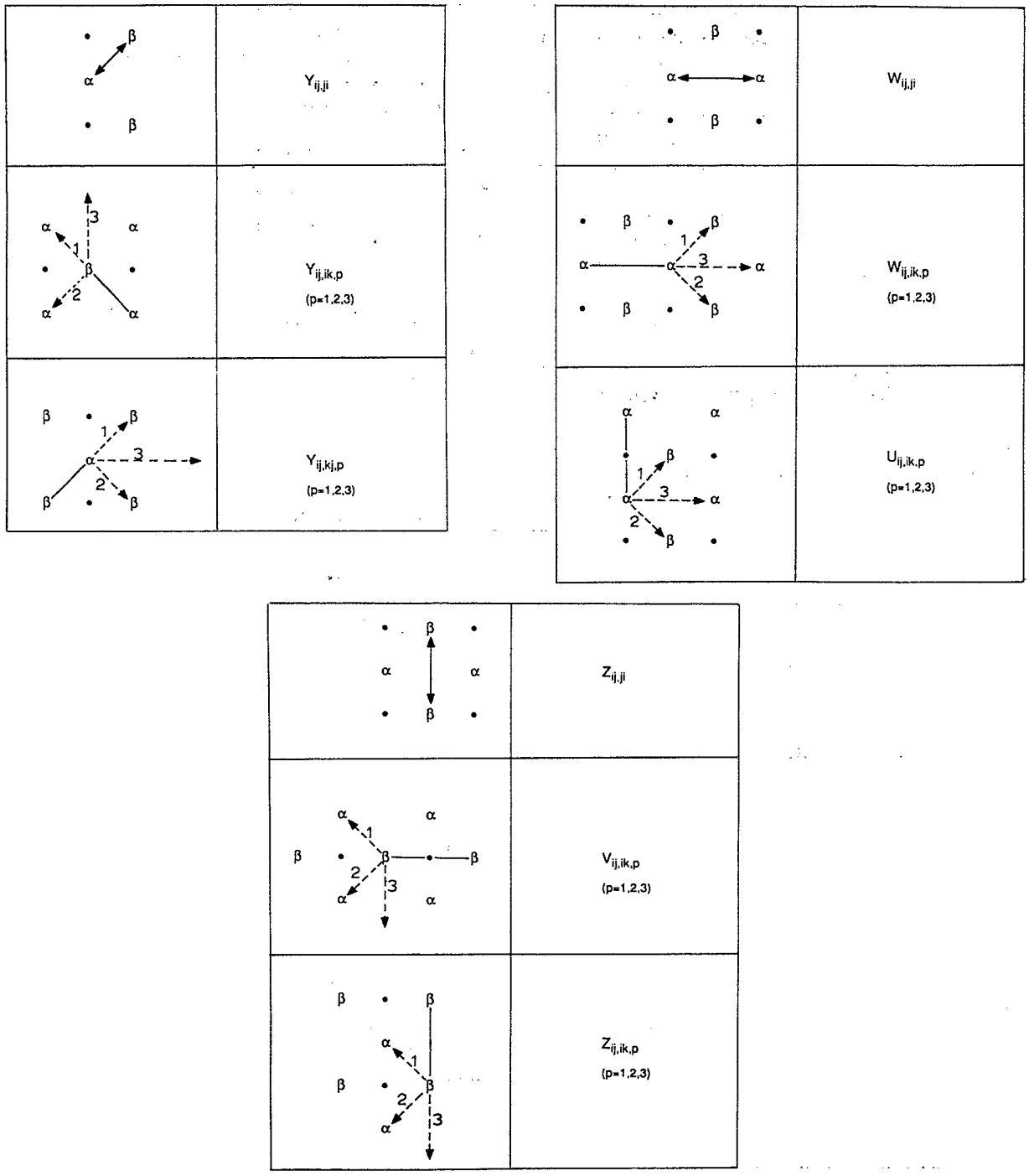

Here $\mathcal{P}_1$ is the number of ways of arranging paths; $\mathcal{P}_2$ is the probability of atomic jumps to the neighboring sites within a time interval Δt; U_{I} and U_{II} are the activation energies for the first- and the second-NN jumps, respectively; θ_{I} and θ_{II} are the number of atomic attempts to jump to the first- and the second-NN sites, respectively; and $\mathcal{P}_3$ is the probability of atomic bonds being broken before oxygen atoms jump to the neighboring sites.

C. The most probable path

The most probable path can be obtained by maximizing the path probability function. In doing so, we keep the variables consistent with each other. This is achieved by maintaining the reduction relations among the variables and by choosing the independent variables in such a way that the reduction relations are always satisfied. Appendixes A and B describe the reduction relations and the derivation of the auxiliary variables. Here, we notice that auxiliary variables α, β, γ, δ, and ζ are defined for the sake of convenience.

The most probable path can be derived by following the procedure described in the following: (i) Differentiate $\ln\mathcal{P}$ with respect to the variables α, β, γ, δ, and ζ. (ii) Using the results obtained in (i), differentiate $\ln\mathcal{P}$ with respect to the independent variables $Y_{ij,ji}$, $Z_{ij,ji}$, and $W_{ij,ji}$.

In order to treat the problems of directional oxygen flux under a chemical potential gradient, $\nabla\mu$, and thus derive the diffusion properties, it is necessary to index the variables to show the position perpendicular to the chemical potential gradient as defined in Fig. 2. The expressions for the most probable path are written as follows:

$$Y_{12,21}^{(2v)}=(\Delta t\theta_{\mathrm{I}})\exp(-U_{\mathrm{I}}/kT)y_{12}^{(2v)}K_{(2v,+)}\ , \tag{3.4}$$

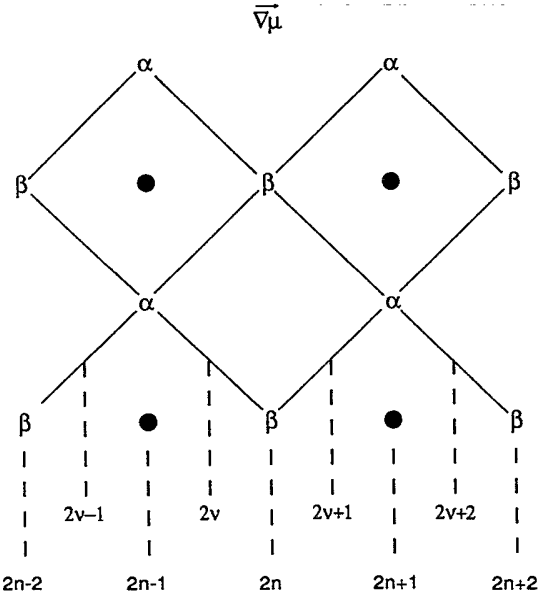

FIG. 2. Schematic illustration of the positions of the lattice planes. The chemical potential gradient is applied perpendicular to the lattice planes.

$$Y_{21,12}^{(2v)}=(\Delta t\theta_{\mathrm{I}})\exp(-U_{\mathrm{I}}/kT)y_{21}^{(2v)}K_{(2v,-)}\ , \tag{3.5}$$

$$W_{12,21}^{(2n)}=(\Delta t\theta_{\mathrm{II}})\exp(-U_{\mathrm{II}}/kT)w_{12}^{(2n)}R_{(2n,+)}\ , \tag{3.6}$$

and

$$W_{21,12}^{(2n)}=(\Delta t\theta_{\mathrm{II}})\exp(-U_{\mathrm{II}}/kT)w_{21}^{(2n)}R_{(2n,-)}\ . \tag{3.7}$$

These are probabilities for oxygen atoms jumping into adjacent vacancies and are the key kinetic probabilities in describing oxygen diffusion. Another path variable $Z_{12,21}$ does not contribute to the net flux in the direction of the chemical potential gradient and, thus, is neglected. Also, we assume that the atomic jump through the Cu atom does not take place.

In the preceding expressions for Y's and W's, the last factors are the probabilities of atomic bonds being broken before an oxygen atom jumps to neighboring sites, and they are defined as follows:

$$\begin{aligned}
K_{(2v,+)}&=\Lambda_{(2v-1),l}^2\Lambda_{(2v),r}\Gamma_{(2n-1),a}^2\Gamma_{(2n-2),l}\Gamma_{(2n),r}\ ,\\
K_{(2v,-)}&=\Lambda_{(2v+1),r}^2\Lambda_{(2v),l}\Gamma_{(2n),a}^2\Gamma_{(2n-l),l}\Gamma_{(2n+1),l}\ ,\\
R_{(2n,+)}&=\Lambda_{(2v-1),l}^2\Lambda_{(2v),r}^2\Gamma_{(2n-1),a}^2\Gamma_{(2n-2),l}\ ,
\end{aligned} \tag{3.8}$$

and

$$R_{(2n,-)}=\Lambda_{(2v+2),r}^2\Lambda_{(2v+1),l}^2\Gamma_{(2n+1),a}^2\Gamma_{(2n+2),r}\ ,$$

where

$$\begin{aligned}
\Lambda_{(2v),r}&=\sum_j\exp(V_{1,1j}/kT)y_{1j}^{(2v)}/x_{\alpha,(2n-1),1}\ ,\\
\Lambda_{(2v),l}&=\sum_j\exp(V_{1,1j}/kT)y_{j1}^{(2v)}/x_{\beta,(2n),1}\ ,\\
\Lambda_{(2v+1),r}&=\sum_j\exp(V_{1,1j}/kT)y_{j1}^{(2v+1)}/x_{\beta,(2n),1}\ ,\\
\Lambda_{(2v+1),l}&=\sum_j\exp(V_{1,1j}/kT)y_{1j}^{(2v+1)}/x_{\alpha,(2n+1),1}\ ,\\
\Gamma_{(2n),a}&=\sum_j\exp(V_{3,1j}/kT)z_{1j}^{(2n)}/x_{\beta,(2n),1}\ ,\\
\Gamma_{(2n),r}&=\sum_j\exp(V_{3,1j}/kT)w_{1j}^{(2n)}/x_{\alpha(2n-1),1}\ ,\\
\Gamma_{(2n),l}&=\sum_j\exp(V_{3,1j}/kT)w_{j1}^{(2n)}/x_{\alpha,(2n+1),1}\ ,\\
\Gamma_{(2n+1),a}&=\sum_j\exp(V_{2,1j}/kT)u_{1j}^{(2n+1)}/x_{\alpha(2n+1),1}\ ,\\
\Gamma_{(2n+1),r}&=\sum_j\exp(V_{2,1j}/kT)v_{1j}^{(2n+1)}/x_{\beta,(2n),1}\ ,
\end{aligned} \tag{3.9a}$$

and

$$\Gamma_{(2n+1),l}=\sum_j\exp(V_{2,1j}/kT)v_{j1}^{(2n+1)}/x_{\beta,(2n+2),1}\ .$$

As was mentioned in Sec. II A only oxygen-oxygen pairs contribute to the interaction energy, so that, for example, one of the expressions of Eq. (3.9a) can be explicitly written as

$$\Gamma_{(2n+1),a}=[u_{11}^{(2n+1)}\exp(V_{2,11}/kT)+u_{12}^{(2n+1)}]/x_{\alpha,(2n+1),1}\ . \tag{3.9b}$$

This expression has an easy interpretation. That is, on one end of a bond, we know an oxygen exists. The factor $u_{11}^{(2n+1)}/x_{\alpha,(2n+1),1}$ is the conditional probability of finding an oxygen next to the known oxygen. The exponential factor by which it is multiplied is the probability that the energy needed to break the bond is concentrated on the bond. Note that $V_{2,11}<0$, so that the stronger the bond, the smaller this exponential factor becomes. The second term, $u_{12}^{(2n+1)}/x_{\alpha,(2n+1),1}$, is the conditional probability of finding a vacancy next to the known oxygen.

The Λ's are for the first-NN bonds and are similarly interpreted. When we know the meaning of Λ's and Γ's, we can understand the structure of the K and R factors in Eq. (3.8). The first quantity $K_{(2\nu,+)}$ in Eq. (3.8) is for a 2ν NN bond, and the subscript $+$ indicates that an oxygen jumps to the $+$ direction, namely from the α end point on $2n-1$ to the β end point on $2n$. As the oxygen jumps from the α, bonds may be broken on the two $2\nu-1$ bonds and on one 2ν bond. The jump occurs at one of the 2ν bonds and, thus, does not contribute to the bond-breaking factor. The number of second-NN bonds to be broken is four: two α-Cu-α bonds at $2n-1$, one α-α bond whose center is at $2n-2$, and another one with the center at $2n$. These four second-NN bonds contribute to the four Γ factors in $K_{(2\nu,+)}$. Other K and R's can be similarly interpreted.

D. Oxygen diffusion flux

The flux expression is derived for a system in which a small chemical potential gradient, $\nabla\mu$, is imposed on the steady state, and where the state variables do not change in time. When the chemical potential gradient, $\nabla\mu$, is small, we expect that $Y_{ij,ji}$ and $W_{ij,ji}$ deviate from the equilibrium value Y_e and W_e, respectively, by the amounts proportional to $\nabla\mu$. We can express the net flux toward the right direction as

$$J_Y^{(2n)}=(Y_{12,21}^{(2\nu)}-Y_{21,12}^{(2\nu)}-Y_{12,21}^{(2\nu+1)}+Y_{21,12}^{(2\nu+1)})/\Delta t$$
$$=Y_e\delta\ln\left[\frac{Y_{12,21}^{(2\nu)}Y_{21,12}^{(2\nu+1)}}{Y_{21,12}^{(2\nu)}Y_{12,21}^{(2\nu+1)}}\right] \tag{3.10}$$

and

$$J_W^{(2n)}=(W_{12,21}^{(2n)}-W_{21,12}^{(2n)})/\Delta t$$
$$=W_e\delta\ln\left[\frac{W_{12,21}^{(2n)}}{W_{21,12}^{(2n)}}\right]\Big/\Delta t\ . \tag{3.11}$$

In the preceding expressions, the subscript e indicates the values in the equilibrium condition and δ is a quantity proportional to the magnitude of $\nabla\mu$.

To expand the parts in large parentheses in Eqs. (3.10) and (3.11), we use the following relationship:[36]

$$f^{(n+\eta)}=f^{(n)}+\eta\frac{df^{(n)}}{dn}\ , \tag{3.12}$$

and apply the definition of the chemical potential μ, written as

$$\mu=\frac{\partial F}{\partial\rho}=2\left[\frac{\partial F}{\partial x_{\alpha,1}}\right]\ . \tag{3.13}$$

The relations in Eqs. (3.10) and (3.11) then transform into the following:

$$J_Y\Delta t=Y_e\left[\delta\ln\frac{y_{12}^{(2\nu)}y_{21}^{(2\nu+1)}}{y_{21}^{(2\nu)}y_{12}^{(2\nu+1)}}-\frac{d}{dn}(\mu/kT)\right] \tag{3.14}$$

and

$$J_W\Delta t=W_e\left[\delta\ln\frac{w_{12}^{(2n)}}{w_{21}^{(2n)}}-\frac{d}{dn}(\mu/kT)\right]\ . \tag{3.15}$$

The total flux $J_{\rm tot}$ is written by using these two equations as

$$J_{\rm tot}^{(2n)}\Delta t=(2J_Y^{(2n)}+J_W^{(2n)})\Delta t$$
$$=2Y_e\delta\hat{y}+W_e\delta\hat{w}-(2Y_e+W_e)\frac{d}{dn}(\mu/kT)\ , \tag{3.16}$$

where

$$\delta\hat{y}=\delta\ln\frac{y_{12}^{(2\nu)}y_{21}^{(2\nu+1)}}{y_{21}^{(2\nu)}y_{12}^{(2\nu+1)}} \tag{3.17}$$

and

$$\delta\hat{w}=\delta\ln\frac{w_{12}^{(2n)}}{w_{21}^{(2n)}}\ . \tag{3.18}$$

In order to convert the δ notation to the gradient of chemical potential, it is convenient to approximate a pair variable expressed as the product of two point variables. For example, $y_{12}^{(2\nu)}\sim x_{\alpha,1}^{(2n-1)}x_{\beta,2}^{(2n)}$. Then, if we apply Eq. (3.12) again and use the relationship $\rho\,d\mu\cong kT\,d\rho$, each of $\delta\hat{y}$ and $\delta\hat{w}$ can be transformed into $-(2/kT)d\mu/dn$. Therefore, the expression of the total flux can be written as

$$J_{\rm tot}\Delta t=-3(2Y_e+W_e)\frac{d}{dn}(\mu/kT)\ . \tag{3.19}$$

To compare this expression with the experimental data, it is necessary to convert the chemical potential gradient, $d\mu/dn$, to the concentration gradient, dC/dx, where C is the number of atoms per cm^3. As this conversion does not require high accuracy, we follow the relationship between the chemical potential gradient and the concentration gradient as derived in our previous calculation,[37] which is now written as

$$\frac{d\mu}{dn}\cong 10^{-14}\frac{1}{x_{\alpha,1}}\frac{dC}{dx}\ . \tag{3.20}$$

Then, we can write the diffusion coefficient expressions (in cm^2/sec) of oxygen by combining Eqs. (3.19) and (3.20) as

$$D=3\times10^{-14}(2Y_e+W_e)/(x_{\alpha,1,e}\Delta t)$$
$$=3\times10^{-14}[2\theta_{\rm I}\exp(-U_{\rm I}/kT)y_{12,e}K_e$$
$$+\theta_{\rm II}\exp(-U_{\rm II}/kT)w_{12,e}R_e]/x_{\alpha,1,e}\ . \tag{3.21}$$

IV. RESULTS

A. Interaction energy parameters

For the equilibrium calculation in Sec. II, we adopted the interaction energy ratios obtained from Sterne's first principle calculation.[38] Figure 3 represents the phase diagram showing oxygen ordering in the Cu-O basal plane of $YBa_2Cu_3O_{7-x}$. Open circles in this figure represent the experimental data obtained by Specht *et al.*[25] and the broken line is calculated by the CVM. By fitting the broken line obtained from the equilibrium calculation to the open circles, we can determine the interaction energy parameter, V_i, between oxygen atoms. Here we assume that oxygen-vacancy and vacancy-vacancy interactions are negligible. The chosen values are $V_1=(V_{1,11})=0.12$, $V_2=-0.04$, and $V_3=0.017$ eV. In addition to these values, we may also consider a different set of energy parameters used in our previous phase diagram calculation,[32] i.e., $V_1=0.09$, $V_2=-0.2$, and $V_3=0.05$ eV. For the sake of convenience, we call the former set V-I and the latter V-II. It is notable that V_1 is the largest value in the V-I set whereas V_2 is the dominant value in the V-II set.

B. Diffusion coefficient

In the present calculation we assume that the atomic flux of the first-NN jump, $Y_{12,21}$, provides the main contribution to the total flux, J_{tot}, and the flux component of the second-NN jump, $W_{12,21}$ is negligible. Figure 4 shows the variation of the oxygen diffusion coefficient with respect to the oxygen content when we apply the V-I energy set. To make the calculated values comparable with the experimental data obtained by Tu *et al.*,[22] we assume $\theta_I \cong 10^9$ and $U_I \cong 0.9$ eV. Even though the lattice parameters change during the phase transformation and thus affect the values of θ_I and U_I, the qualitative properties of this curve may not be substantially affected. In this figure, we note that the derivative of the diffusion coefficient with respect to the oxygen content is not continuous at the phase transition point and the left- and the right-hand sides of the transition point represent the tetragonal and the orthorhombic regions, respectively. The oxygen diffusion coefficient increases with a decrease of oxygen content in the orthorhombic region. But in the tetragonal region, the oxygen diffusion coefficient changes with an opposite trend, i.e., it decreases slowly as the oxygen content decreases.

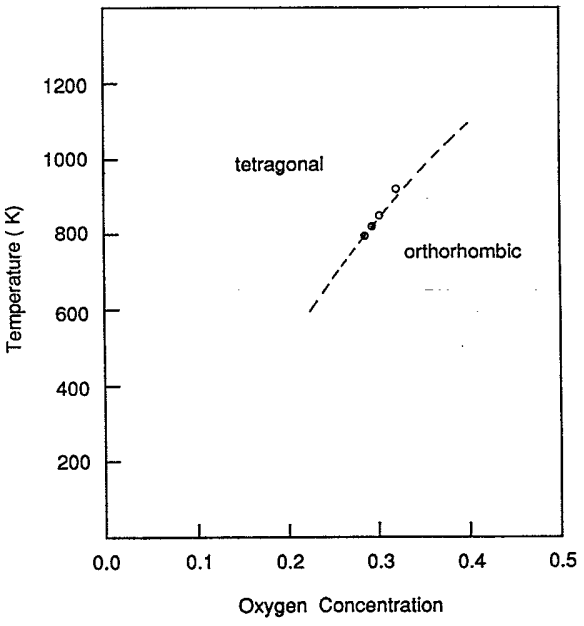

FIG. 3. Phase diagram showing oxygen ordering in the Cu-O basal plane. The calculation was done by employing the pair approximation of the CVM. The chosen energy parameters are $V_1=0.12$, $V_2=-0.04$, and $V_3=0.017$ eV. Open circles are experimental data obtained by Specht *et al.* (Ref. 25).

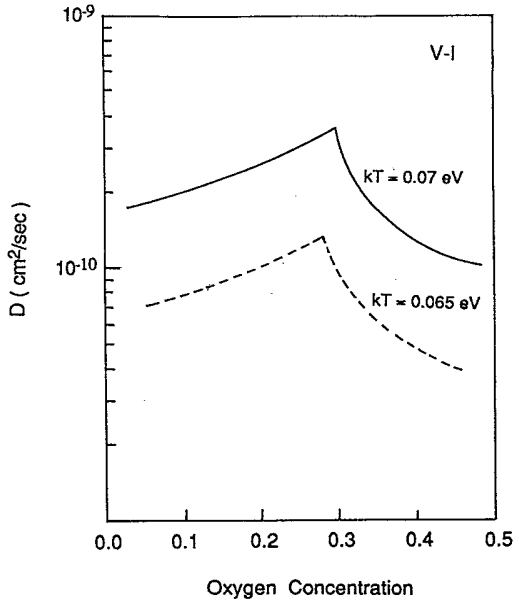

FIG. 4. Variation of the oxygen diffusion coefficient with respect to oxygen content when the V-I energy set is applied.

In Eq. (3.21), θ_I and U_I are independent of the oxygen content but $y_{12,e}$ and K_e are dependent. Figure 5 shows the variation of $y_{12,e}$, $Y_{11,e}$ for the NN pairs and $u_{11,e}$ for the O-Cu-O superexchange pairs with respect to the oxygen content at $kT=0.07$ eV. From this figure, it can be noted that the bond-breaking factor, K_e, plays a dominant role in determining the diffusion coefficient in the orthorhombic region.

The number of O-Cu-O pairs, which have an attractive interaction energy, decreases rapidly with a decrease in oxygen content making the $u_{12,e}$ for the oxygen-vacancy pair more important in $\Gamma_{(2n+1),a}$ of Eq. (3.9a); thus, the K_e value increases sharply. In the tetragonal region, however, oxygen atoms are more randomly distributed and the bond-breaking factor does not change very much in this region because of the small value of V_2 in the V-I energy category. Hence, the oxygen-vacancy pair probability, $y_{12,e}$ plays an important role in this region and the oxygen diffusion coefficient follows the trend of $y_{12,e}$ variation.

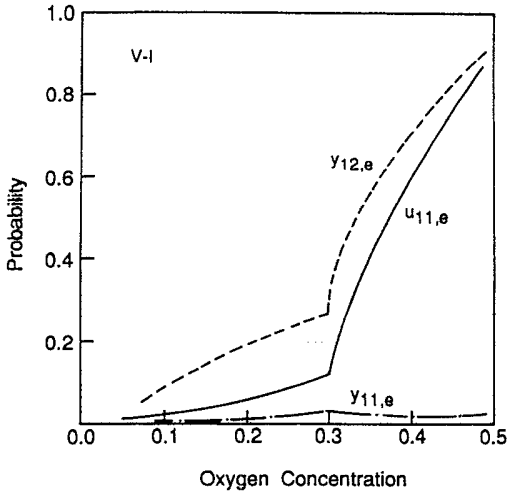

FIG. 5. Profiles of the pair probabilities with respect to oxygen content when the V-I energy set is applied ($kT=0.07$ eV).

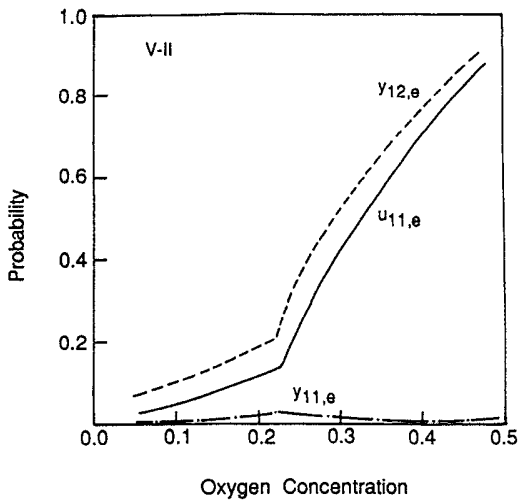

FIG. 7. Profiles of the pair probabilities with respect to oxygen content when the V-II energy set is applied ($kT=0.08$ eV).

When the V-II energy set is applied, the oxygen diffusion coefficient with respect to oxygen content displays a different trend as shown in Fig. 6. In this figure, oxygen diffusion values are plotted on a relative scale and we notice that, even in the tetragonal region, the diffusion coefficient increases with decreasing oxygen content.

Figure 7 represents $y_{12,e}$, $y_{11,e}$, and $u_{11,e}$ plotted against the oxygen content when the V-II energy set is applied. In the V-II energy parameter, it is noted that the absolute value of the V_2/V_1 ratio is larger than 1.0 and the bond-breaking factor is more sensitive to the number of O-Cu-O pairs rather than that of the first-NN O-O pairs. For this reason, the trend of the oxygen diffusion coefficient is determined by the variation of $u_{11,e}$ in both the tetragonal and orthorhombic regions. The general feature of the oxygen diffusion coefficient is that the oxygen diffusion in the disordered phase is faster than that in the ordered phase, and the oxygen diffusion coefficient increases sharply as the second-order transition point is approached from the orthorhombic phase.

In Fig. 8, the logarithm of the diffusion coefficient is plotted against the reciprocal temperature at a fixed chemical potential value ($\mu=0.12$ eV), using the V-I energy set. We note that the curves roughly correspond to two linear potentials, and the activation energies, obtained by measuring the slope of each linear portion, are 0.8 and 1.2 eV for the tetragonal and orthorhombic phases, respectively.

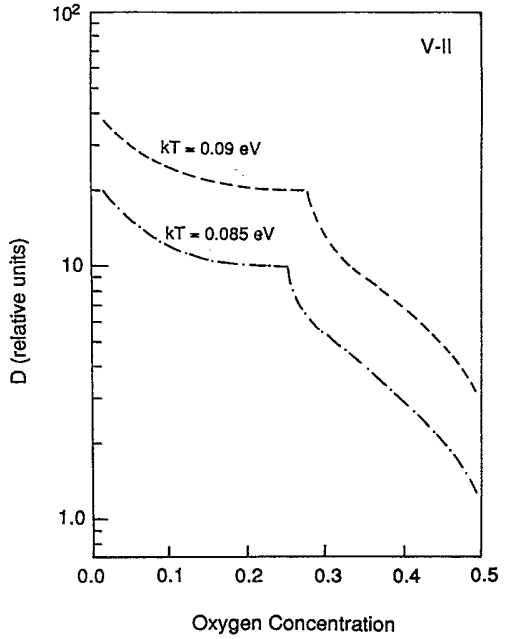

FIG. 6. Variation of the oxygen diffusion coefficient with respect to oxygen content when the V-II energy set is applied.

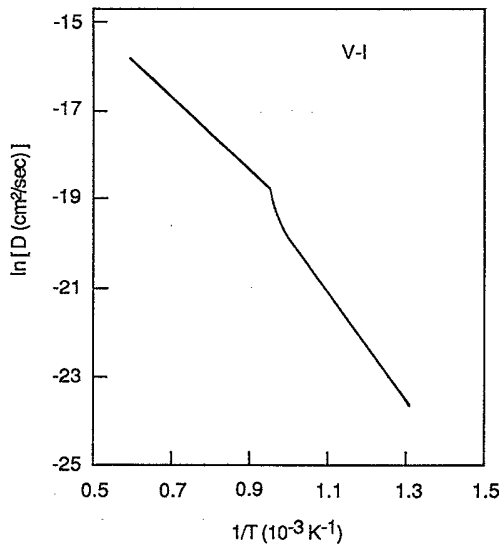

FIG. 8. Logarithm of the diffusion coefficient plotted with respect to the reciprocal temperature when the V-I energy set is applied (μ is fixed at 0.08 eV).

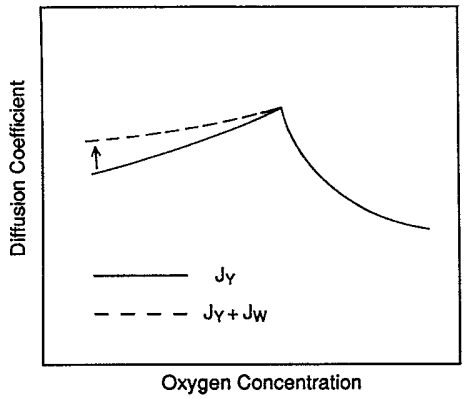

FIG. 9. Schematic diagram of the oxygen diffusion coefficient plotted against oxygen content. The broken line represents a possible contribution of the J_W component to the total flux.

When we compare the present results obtained through modeling with the experimental data published in the literature, it is appropriate to consider the effect of transformation twins in the lattice and their orientations with respect to the diffusion direction chosen. This is because our recent calculation[31] shows that the oxygen diffusion rate near and at the twin boundary is much faster than that in the bulk orthorhombic region.

C. Comments on atomic flux of the second-NN jump

In the calculation of the diffusion coefficient, we assumed that the J_Y component provides the main contribution to the total flux. This assumption seems reasonable in the orthorhombic phase where J_W has values from $J_Y/10$ to $J_Y/100$ when we apply the same values of θ_{I} and U_{I} for those of θ_{II} and U_{II}, respectively. But in the tetragonal region, especially toward the lower oxygen content, the J_W component has values comparable with the J_Y component. Even though it is hard to imagine that θ_{II} and U_{II} are comparable with θ_{I} and U_{I}, we should consider the possibility that the oxygen diffusion coefficient curves in the tetragonal region may need to be adjusted to the higher positions, as shown schematically in Fig. 9. In order to confirm that the role of the J_W component in oxygen diffusion is negligible in the orthorhombic structure, it is necessary to measure the rate of oxygen diffusion experimentally for both **a** and **b** directions. If oxygen diffusion rates are equal in each direction, we can conclude that J_W has little effect on J_{tot}.

V. DISCUSSION AND SUMMARY

The physical properties of materials are sensitive to variations in the microstructure. Polycrystalline $YBa_2Cu_3O_{7-x}$ samples are no exception to this rule, and both the superconducting and the mechanical properties should be heavily dependent on the microstructural variations. These features exist on scales in micrometer (such as phase assemblages, grain morphologies, etc.) and macrometer ranges (such as grain and twin boundaries, point defects, and ordering). Although considerable research has been reported in the literature since the discovery of superconductors above 90 K,[39] as yet, there is not a well-established correlation between the macrostructure and the superconducting behavior of $YBa_2Cu_3O_{7-x}$. Nevertheless, the behavior of oxygen in these materials, in modifying microstructures on many scales, appears to have the most dramatic effect. Foremost, as proposed, the high-T_c superconductivity in these compounds is related to the orthorhombic form of $YBa_2Cu_3O_{7-x}$.[1-4] The behavior of oxygen in the microstructure during heat treatment varies depending on the heating, annealing, cooling, and post annealing cycles (with changes in the rate and cooling, nature of the atmosphere, the partial pressures of gases, and holding times).[5,12,22-25] These different conditions result in the inhomogeneous distribution and ordering of oxygen within the grains and grain boundaries of the samples. It appears, therefore, that in order to achieve predictable superconducting properties in $YBa_2Cu_3O_{7-x}$ an understanding of the behavior of oxygen in the compound is required. Along these lines, many theoretical and experimental studies have been performed on the kinetics of oxygen diffusion with considerable variation in activation energies and diffusivities. In this paper, we reported a theoretical study of oxygen diffusion in both the tetragonal and the orthorhombic forms of $YBa_2Cu_3O_{7-x}$ in which experimental and theoretical information was used to carry out the calculations. The intent of the study was to find the parameters related to the oxygen diffusion in a "homogeneous" lattice which would provide a common base for further studies.

In summary, the pair approximation of the PPM was applied to calculate the oxygen diffusion rate in the $YBa_2Cu_3O_{7-x}$ superconducting compound. One first-NN and two second-NN interaction energies were used for the calculation and we assumed that oxygen diffusion occurs mainly in the Cu-O basal plane. It was noted that even when we included the second-NN interaction energy parameters in our calculation, the bond-breaking factor could be expressed analytically, as was done by including only the first-NN interactions in Ref. 36.

We noted from the calculations that the oxygen diffusion coefficients are functions of the oxygen density and the degree of long-range ordering of oxygen-vacancy distribution in the Cu-O basal plane. Oxygen diffusion in the disordered tetragonal phase is faster than that in the ordered phase and it changes sharply near the phase transition point. This is because the fraction of O-Cu-O pairs, which have an attractive interaction, decreases rapidly when the orthorhombic phase transforms to the tetragonal phase. Hence, if the orthorhombic region is kept at a constant temperature, the oxygen diffusion rate increases as the oxygen concentration decreases. The trend of oxygen diffusion in the tetragonal region, however, is dependent on the values of the interaction energy parameters. If the V_1 repulsion (NN) is dominant, the variation in the rate of oxygen diffusion depends on the probability of finding an oxygen-vacancy pair, because the probability of finding the first-NN oxygen-oxygen pair is very small. On the other hand, if the V_2 attraction

in O-Cu-O is dominant, the trend of the oxygen diffusion rate with respect to the oxygen content is determined by the probability of finding the O-Cu-O pair, which controls the bond-breaking factor. In the present study, we assumed that the first-NN atomic jump provides the main contribution to the total flux and the second-NN jump is negligible. But, we cannot exclude the possibility that the latter jump makes a certain contribution to the total flux when the structure is tetragonal.

In this study, it is assumed that the lattice is perfect and, therefore, there are no defects or other microstructural variations which would influence the behavior of oxygen. Therefore, the diffusivities found above are the average for **a** or **b** directions in both lattices, as stated earlier. In reality, however, there are always transformation twins in the microstructure. These twins form on (110) and $(1\bar{1}0)$ planes[40] as a means to accommodate stresses that develop because of the shape change related to oxygen ordering during the transformation from the tetragonal to the orthorhombic phase. It is, therefore, possible that twin boundaries also act as an easy diffusion path, similar to "pipe diffusion" along dislocations. In a planned future paper,[31] we perform a theoretical study of the equilibrium atomic distribution and the oxygen kinetics near the twin boundary in $YBa_2Cu_3O_{7-x}$. The calculations show a large increase in the oxygen diffusion coefficient as the lattice plane approaches the twin boundary. Furthermore, the diffusion of oxygen is closely related to the density profile which shows that oxygen is depleted at the twin boundary region. For a complete understanding of oxygen behavior in a polycrystalline material, however, it would be necessary to study the surface (and grain boundary) diffusion of oxygen in addition to the bulk and twin boundary diffusion.

ACKNOWLEDGMENTS

Discussions with members of the Advanced Ceramic Materials Laboratory of the Washington Technology Centers are gratefully acknowledged. This work was supported by the U. S. Defense Advanced Research Projects Agency (DARPA) and the Air Force Office of Scientific Research (AFOSR) through Boeing Aerospace Co. under Contract No. HB-2121.

APPENDIX A: THE REDUCTION RELATIONS

In this appendix, we describe the reduction relations among the state and the path variables. These reduction relations are used to differentiate the path probability function with respect to independent variables such as $Y_{12,21}$ and $W_{12,21}$. For the sake of simplicity, we consider the components which include $Y_{12,21}$ and neglect other components. Throughout this appendix, the subscript p denotes the atomic path number 1 or 2 in Tables III and IV. From Tables III and IV we can easily write

$$x_{\alpha,i}^{(2n-1)}=X_{\alpha,ii}^{(2n-1)}+\sum_p X_{\alpha,ij,p}^{(2n-1)} ,$$
$$x_{\beta,i}^{(2n)}=X_{\beta,ii}^{(2n)}+\sum_p X_{\beta,ij,p}^{(2n)} , \tag{A1}$$

and

$$y_{11}^{(2v)}=Y_{11,11}^{(2v)}+Y_{11,21,1}^{(2v)} ,$$
$$y_{11}^{(2v-1)}=Y_{11,11}^{(2v)}+\sum_p Y_{11,21,p}^{(2v)}$$
$$y_{12}^{(2v)}=Y_{12,12}^{(2v)}+\sum_p Y_{12,22,p}^{(2v)}+Y_{12,21}^{(2v)} , \tag{A2}$$

and

$$y_{22}^{(2v+1)}=Y_{22,22}^{(2v+1)}+\sum_p Y_{22,21,p}^{(2v+1)} .$$

The relations between the second-NN pairs are written as follows:

$$w_{11}^{(2n)}=W_{11,11}^{(2n)}+\sum_p W_{11,21,p}^{(2n)} ,$$
$$w_{12}^{(2n)}=W_{12,12}^{(2n)}+\sum_p W_{12,22,p}^{(2n)} . \tag{A3}$$

The relations for other variables can be described in a similar way.

APPENDIX B: AUXILIARY VARIABLES

We define the auxiliary variables to maximize the path probability function in a convenient way. In this appendix, we describe how to define the auxiliary variables, α, β, γ, δ, and ζ, and how they are used. As an example, we consider a variable $\alpha_{11,21,p}^{(2v-1)}$ which satisfies

$$Y_{11,21,p}^{(2v-1)}=\tfrac{1}{2}(Y_{12,21}^{(2v)}+\alpha_{11,21,p}^{(2v-1)}) ,$$
$$Y_{12,22,p}^{(2v-1)}=\tfrac{1}{2}(Y_{12,21}^{(2v)}-\alpha_{11,21,p}^{(2v-1)}) . \tag{B1}$$

The differentiation of $N^{-1}\ln\mathcal{P}$ with respect to $\alpha_{11,21,p}$ leads to the following relation:

$$\frac{Y_{11,21,p}^{(2v-1)}}{\exp(V_1/kT)y_{11}^{(2v-1)}}=\frac{Y_{12,22,p}^{(2v-1)}}{y_{12}^{(2v-1)}}=k_1=\text{const.} \tag{B2}$$

From Table IV,

$$Y_{12,21}^{(2v)}=Y_{11,21,p}^{(2v-1)}+Y_{12,22,p}^{(2v-1)} . \tag{B3}$$

If we substitute Eq. (B2) for Eq. (B3) we get

$$Y_{11,21,p}^{(2v-1)}=\frac{\exp(V_1/kT)y_{11}^{(2v-1)}}{\exp(V_1/kT)y_{11}^{(2v-1)}+y_{12}^{(2v-1)}}Y_{12,21}^{(2v)} ,$$
$$Y_{12,22,p}^{(2v-1)}=\frac{y_{12}^{(2v-1)}}{\exp(V_1/kT)y_{11}^{(2v-1)}+y_{12}^{(2v-1)}}Y_{12,21}^{(2v)} . \tag{B4}$$

In a similar way, the relationship between $\Phi_{ij,ik,p}$ and independent variables of which the subscripts are the ij,ji type can be derived. Here Φ represents the Y, W, U, V, and Z variables.

*Present address: Department of Materials Science and Engineering, University of California, Los Angeles, Los Angeles, CA 90024.

[1]J. D. Jorgensen, B. W. Veal, W. K. Kwok, G. W. Crabtree, A. Umezawa, L. J. Nowicki, and A. P. Paulikas, Phys. Rev. B **36**, 5731 (1987).

[2]I. K. Schuller, A. G. Hinks, M. A. Beno, S. W. Capone II, L. Sodelholm, J.-P. Locquet, Y. Bruynseraede, C. U. Segre, and K. Zhang, Solid State Commun. **63**, 365 (1987).

[3]J. M. Tarascon, L. H. Greene, B. G. Bagley, W. R. McKinnon, P. Barboux, and G. W. Hall, in *Proceedings of the International Workshop on Novel Superconductivity,* edited by V. Kresin and S. Wolf (Pergamon, New York, 1987), p. 705.

[4]R. J. Cava, B. Batlogg, C. Chen, E. A. Rietman, S. M. Zahurak, and D. Werder, Phys. Rev. B **36**, 5719 (1987).

[5]Y. Kubo, T. Yoshitake, J. Tabuchi, Y. Nakabayashi, A. Ochi, K. Utsumi, H. Igarashi, and M. Yonezawa, Jpn. J. Appl. Phys. **26**, L768 (1987).

[6]R. Beyers, G. Lim, E. M. Engler, V. Y. Lee, M. L. Ramirez, R. J. Savoy, R. D. Jacowitz, T. M. Shaw, S. LaPlaca, R. Boehme, C. C. Tsuei, S. I. Park, M. W. Shafer, W. J. Gallagher, and G. V. Chandrashekhar, Appl. Phys. Lett. **51**, 614 (1987).

[7]Y. Saito, T. Noji, A. Endo, N. Matsuzaki, M. Katsumata, and N. Higuchi, Jpn. J. Appl. Phys. **26**, L491 (1987).

[8]See, for example, J. Bardeen, in *Proceedings of the International Workshop on Novel Superconductivity,* Ref. 3, p. 500.

[9]H. You, J. D. Axe, X. B. Kan, S. C. Moss, J. L. Liu, and D. J. Lam, Phys. Rev. B **37**, 2301 (1988).

[10]Z. Hiroi, M. Takano, Y. Ikeda, Y. Takeda, and Y. Bando, Jpn. J. Appl. Phys. **27**, L141 (1988).

[11]M. Sarikaya and E. A. Stern, Phys. Rev. B **37**, 9373 (1988).

[12]D. G. Gintey, E. L. Venturini, J. F. Kwok, R. J. Baughman, and B. Morrison, J. Mater. Res. **4**, 496 (1989).

[13]A. Robledo and C. Varea, Phys. Rev. B **37**, 631 (1988).

[14]G. J. Dolan, G. V. Chandrashekhar, T. R. Dinger, C. Feild, and F. Holzberg, Phys. Rev. Lett. **62**, 827 (1987).

[15]D. Dimos, P. Chandhari, J. Mannhart, and F. K. LeGoues, Phys. Rev. Lett. **61**, 219 (1988).

[16]S. E. Babcock and D. C. Larbalestier, Appl. Phys. Lett. **55**, 393 (1989).

[17]See, for example, M. Hervieu, B. Domenges, C. Michel, G. Herger, J. Provost, and B. Raveau, Phys. Rev. B **36**, 3920 (1980).

[18]A. G. Khachaturyan and J. W. Morris, Jr., Phys. Rev. Lett. **61**, 215 (1988).

[19]C. H. Chen, D. J. Werder, R. J. Cava, L. F. Schneemayer, B. Batlogg, and A. K. Gallagher, in *High Temperature Superconductors–II,* edited by D. W. Capone II, W. H. Butler, B. Batlogg, and C. W. Chu (Materials Research Society, Pittsburgh, PA, 1988), p. 35.

[20]G. Deutscher and K. A. Müller, Phys. Rev. Lett. **59**, 1745 (1987).

[21]S. Viera, P. Zhou, S. A. Solin, N. Garcia, M. Hortal, and A. Aguilo, Phys. Rev. B **39**, 339 (1989).

[22]K. N. Tu, N. C. Yeh, S. I. Park, and C. C. Tsuei, Phys. Rev. B **39**, 304 (1989).

[23]E. Saiz and J. S. Moya, Mater. Lett. **6**, 369 (1988).

[24]J.-H. Park, P. Kostic, and J. P. Singh, Mater. Lett. **6**, 393 (1988).

[25]E. D. Specht, C. J. Sparks, A. G. Dhere, J. Brynestad, O. B. Cavin, D. M. Kroeger, and H. A. Oye, Phys. Rev. B **37**, 7426 (1988).

[26]H. Bakker, J. P. A. Westerveld, D. M. R. Lo Cascio, and D. O. Welch, Physica C **157**, 25 (1989).

[27]J. Zhang, M. Yang, and T. Chen, Mater. Lett. **6**, 379 (1988).

[28]Y. Ikuma and S. Akiyoshi, J. Appl. Phys. **64**, 391 (1988).

[29]Y. Song, X.-D. Chen, and J. R. Gaines, J. Mater. Res. **5**, 27 (1990).

[30]R. J. Borg and G. J. Dienes, *An Introduction to Solid State Diffusion* (Academic, Boston, 1988), p. 139.

[31]J.-S. Choi, M. Sarikaya, I. A. Aksay, and R. Kikuchi (unpublished).

[32]R. Kikuchi and J.-S. Choi, Physica C **160**, 347 (1989).

[33]R. Kikuchi, Phys. Rev. **81**, 988 (1951).

[34]R. Kikuchi, Prog. Theor. Phys. Suppl. **35**, 1966.

[35]R. Kikuchi and H. Sato, J. Chem. Phys. **60**, 1071 (1974).

[36]R. Kikuchi, J. Chem. Phys. **51**, 161 (1969).

[37]R. Kikuchi and J.-S. Choi (unpublished).

[38]P. Sterne (private communication).

[39]M. K. Wu, J. R. Ashburn, C. J. Torng, P. H. Hor, R. L. Meng, L. Gao, Z. J. Huang, Y. Q. Wang, and C. W. Chu, Phys. Rev. Lett. **58**, 908 (1987).

[40]M. Sarikaya, R. Kikuchi, and I. A. Aksay, Physica C **152**, 161 (1988).